10TH INTERNATIONAL SYMPOSIUM ON PARTICLE IMAGE VELOCIMETRY – PIV13
Delft, The Netherlands, July 1-3, 2013

Complete removal of ghost particles in Tomographic-PIV

G.E. Elsinga

Laboratory for Aero & Hydrodynamics, Department of Mechanical, Maritime and Materials Engineering,
Delft University of Technology, Delft, The Netherlands
g.e.elsinga@tudelft.nl

ABSTRACT
This paper discusses and compares several methods, which aim to remove spurious peaks, i.e. ghost particles, from the volume intensity reconstruction in Tomographic-PIV. The assessment is based on numerical simulations of time-resolved tomographic-PIV experiments in linear shear flows. Within the reconstructed volumes intensity peaks are detected and tracked over time. These peaks are associated to particles (either ghosts or actual particles) and are characterized by their peak intensity, their size and their track length. Peak intensity and track length are found to be effective in discriminating between most ghosts and the actual particles, although not all ghosts can be detected using only a single threshold. The size of the reconstructed particles does not reveal an important difference between ghosts and actual particles. Simultaneous plotting of peak intensity and track length however does, under certain conditions, allow a complete separation of ghosts and actual particles. The ghosts can have either a high intensity or a long track length, but not both combined like all the actual particles. Finally removing the detected ghosts from the reconstructed volume and performing additional MART iterations can decrease the particle position error at low to moderate seeding densities, but increases the position error and tracking errors at higher densities.

1. INTRODUCTION

Tomographic PIV (Elsinga et al. 2006a) has proven to be a useful tool for measuring three-dimensional fluid velocity fields and examining the flow structures, like for example vortices. Overviews of applications and subsequent developments are given in Scarano (2013) and Westerweel et al. (2013). A critical processing step determining the accuracy of the final velocity field seems to be the tomographic reconstruction of the tracer particle distribution within the measurement volume. Unfortunately, the means to assess the accuracy of a reconstructed volume are limited in an actual experiment. This is simply because the true particle distribution is unknown. Therefore, current practice is to consider the average reconstruction intensity inside and outside light sheet as a measure of the overall reconstruction accuracy (Elsinga et al. 2006a,b). While useful, this does not detect the location of the spurious intensity peaks in the reconstruction, known as ghost particles (Maas et al. 1993, Elsinga et al. 2011), which comprise the reconstruction noise. More elaborate approaches have recently been introduced to detect some of these ghosts and remove them from the reconstructions (Novara et al. 2010, de Silva et al. 2013). This has been shown to reduce noise in the final velocity field. Remaining ghosts can, however, still create a bias error (Elsinga et al. 2011), which is more difficult to detect, or even correct.

Furthermore, Schröder et al. (2011) proposed to use the tomographic reconstructions of the tracer particle distributions to perform particle tracking and obtain particle accelerations. Before, such acceleration measurements were performed by 3D-PTV (e.g. La Porta et al. 2001). Compared to 3D-PTV the use of Tomographic PIV would in principle allow for an increase in particle density by at least an order of magnitude. However, with this advantage comes the introduction of false, or ghost, particles, which may bias acceleration statistics.

Ghosts thus negatively affect the measurement accuracy of both velocity and particle acceleration. Therefore, it is of interest to investigate whether all ghost particles can be detected and removed in a given experiment. Previous attempt at removing ghosts were certainly successful, but were never able to indicated the percentage of ghost that were actually removed. In other words: a method for convincingly showing whether all ghosts can be removed in an actual experiment does not yet exist. The aim of this work is thus to develop such a method, based on which it will be possible to determine the experimental conditions allowing completely separating the ghosts from the actual particles without ambiguity.

Given our interest in the time evolution of (turbulent) flows and increasing the yield of acceleration measurements, we will consider mainly time-resolved Tomographic-PIV in this investigation. Indeed, separating out all ghosts in dual exposure Tomographic-PIV will be much harder to accomplish, as discussed below. Furthermore, the method for ghost detection and separation needs to be based on an a-posteriori evaluation of the measurement. This is needed, because

some of the properties of ghost particles depend on the actual flow and exact distribution of tracer particles, which is not known beforehand usually.

We proceed by discussing the known properties of ghost particles and existing methods for detecting ghosts (section 2). The discriminating power of each of these properties is investigated using numerical simulations of a time-resolved Tomographic-PIV experiment in a shear flow. Then by combining these insights a criterion for complete separation of ghosts is obtained (section 3), which will be used to enhance the tomographic reconstruction (section 4). The effectiveness of different ghost detection methods and other main findings are discussed and summarized in section 5.

2. DISCRIMINATING POWER OF EXISTING GHOST DETECTION METHODS

The existing methods for ghost detection will be reviewed based on a set of numerical simulations of a time-resolved Tomographic-PIV experiment. The layout of these simulations is analogue to what was used before in Elsinga et al. (2006a, 2011). In particular, the measurement volume is represented by a 2D slice of 1000 voxels in length (corresponding to the x-direction) and 200 voxels in depth (z-direction). Then the particle images are recorded from four different viewing directions onto 1D pixel lines containing 1000 pixels each. The viewing directions are -30, -10, 10 and 30 degrees with respect to the z-direction. Different seeding conditions are achieved by having either about 70, 100 or 150 tracer particles randomly distributed within the measurement volume at any instant in time. These conditions correspond to a particle image density of 0.07, 0.10 and 0.15 particles per pixel in the 1D images, ppp_{1D}, and approximately 0.02, 0.03 and 0.05 ppp in regular 2D images (assuming each particle spans across three slices in a 3D volume). The diameter and the peak intensity of the particle images are constant at 3 pixels and 80 counts respectively. Between consecutive recordings the tracer particles are displaced only in the x-direction according to:

$$\begin{aligned} \Delta x_p &= 10 voxels\left(1-\theta\frac{z_p}{l_z}\right) \\ \Delta z_p &= 0 \end{aligned} \tag{1}$$

where Δx_p and Δz_p are the particle displacements in the x-direction and depth direction respectively in voxel units, z_p is the depth position of the particle in voxel units, and l_z is the depth of volume (200 voxels presently). The resulting displacement field represents a shear flow governed by the parameter θ, which is equal to the percentage difference in velocity across the volume. From the recordings the particle distribution is reconstructed by the MART tomographic algorithm using 5 iterations (Elsinga et al. 2006a).

Within the reconstructed volumes intensity peaks are detected, which are taken to represent particles. The sub-pixel location of each peak is determined from a Gaussian peak fit. By comparing to the true particle distribution ghosts and actual particles can be differentiated. An intensity peak in the reconstructed volume is associated to an actual particle if located within 2.0 voxels of this actual particle. All particles, ghost and actual, are followed over time using a basic tracking approach (Maas et al. 1993). The particle traces are continued by predicting the particle location at the next time instant using the mean particle displacement field and then finding the reconstructed particle closest to the predicted location within a search radius of 2.1 voxels. A trace is discontinued if no matching particle is found within this search radius.

Along each particle trajectory the reconstructed particle properties are determined, which include peak intensity, size and the length over which a particle can be traced. The ghosts are compared to the actual particles based on the statistical distributions of each property. Below results will be presented for a seeding density of ppp_{1D} = 0.07 and a flow velocity variation over the volume of θ = 0.5%, unless indicated otherwise. The seeding density in this baseline configuration can be considered relatively low yielding a high reconstruction quality Q = 0.9. On the other hand the variation in particle displacement across the volume depth is small; over 100 time steps an actual particle will be displaced between 1000 and 995 voxels depending on its location in depth.

The expected peak intensity is lower for a ghost compared to an actual particle, which has been recognized early on (Elsinga et al. 2006a, Atkinson and Soria 2009, Novara 2013). The respective peak intensity distributions for the present simulations are shown in figure 1. It is seen that the intensity of the ghosts is around 10 counts, while the actual particle intensity is 40 counts typically. Still the intensity distributions are found to partially overlap even at this relatively low seeding density. Therefore, a full separation of ghosts and actual particles by intensity thresholding cannot be achieved in this case. In order to achieve separation of intensities the seeding concentration needs to be lowered even further, but the objective here is to maintain relatively high concentrations and still remove all ghosts. Hence, alternative criteria have to be considered.

De Silva et al. (2013) argued that the size of the ghost particles is generally smaller than the reconstructed actual particles. To obtain a measure of the reconstructed particle size they introduce a parameter Gamma, which is basically the sum of the reconstructed intensities in the neighborhood of a particle. A larger particle yields a larger Gamma, but as recognized by the authors, their original Gamma is still sensitive to the intensity of the reconstructed particle. Here, the remaining effect of the particle intensity is removed by normalizing the intensities with the peak intensity before summing over the neighborhood. This will be referred to as the normalized Gamma. The neighborhood in this case is a 5x5 voxels region centered on the intensity peak. The results for the normalized Gamma are presented in figure 2. The ghost and actual particle distributions largely overlap, from which it is concluded that reconstructed particle size has very low discriminating power. Hence, the ability of the original Gamma (de Silva et al. 2013) to remove some ghosts from the reconstruction must be ascribed largely to intensity differences rather than size differences.

A final property used to remove ghosts is the length or time, over which a particle can be traced. In order for a ghost to reappear at subsequent times (allowing it to be tracked in time), it has to be formed from the same set of actual particles, which will happen only if these actual particles are displaced over approximately the same distance (Elsinga et al. 2006b, 2011). However, over time, differences in displacement built up due to velocity variations within the volume, eventually causing the ghost to disappear. It is thus expected that ghosts can be traced over shorter distances compared to actual particle, which in principle never disappear unless they move out of the measurement volume. This principle has, for instance, been used by Schröder et al. (2011) to remove potential ghost trajectories. The employed track length threshold was arbitrarily selected in these studies. The track lengths obtained in the present simulations are presented in figure 3. Indeed, the reconstructed actual particles can be followed over the full length of the measurement domain, i.e. 1000 voxels, while most of the ghosts disappear from the volume before reaching the volume edge. Therefore, the track length can be considered very effective in separating ghosts and actual particles. Nevertheless, some ghost trajectories do span the entire volume length and cannot be distinguished in this way. Even when increasing the velocity variation to $\theta = 5.0\%$, ghost particles can still survive all the way across the volume occasionally.

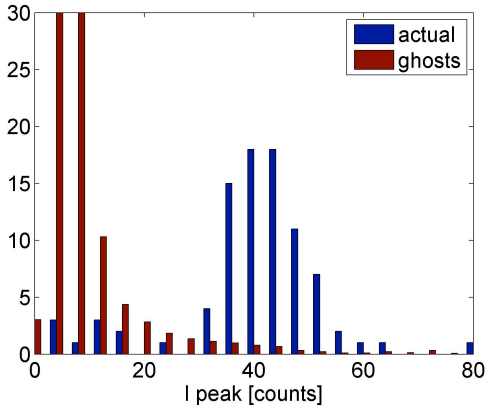

Figure 1. Histogram of particle peak intensity. Results shown are for $ppp_{1D} = 0.07$ and $\theta = 0.5\%$.

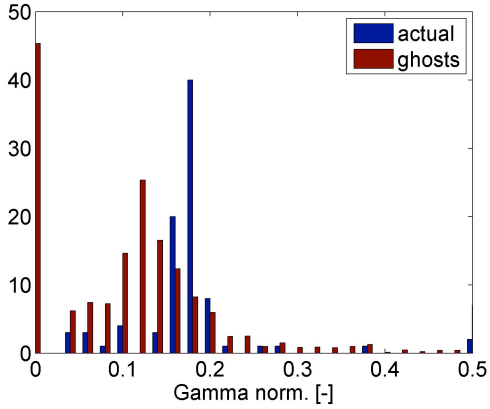

Figure 2. Histogram of normalized Gamma, which is representative of the reconstructed particle size. Results shown are for $ppp_{1D} = 0.07$ and $\theta = 0.5\%$.

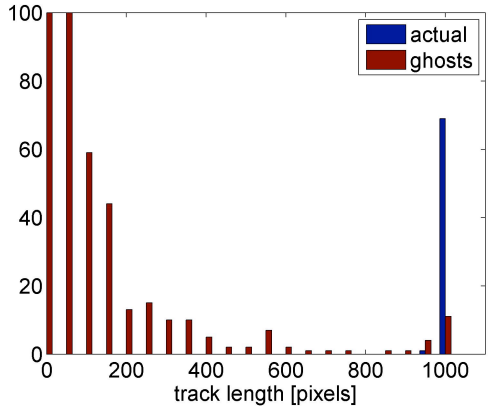

Figure 3. Histogram of particle track length in voxel units. Results shown are for $ppp_{1D} = 0.07$ and $\theta = 0.5\%$.

3. COMPLETE GHOST REMOVAL

Results in the previous section clearly revealed that none of the particle properties could perfectly distinguish ghost and actual particles. In this section, we therefore use different combinations of parameters to achieve a complete separation. Particle intensity and size are always available in any Tomographic-PIV experiment, because they do not require time-resolved measurements. Therefore, the combination of these two properties has the most general applicability. They even fully characterize a reconstructed particle, i.e. an intensity blob in the reconstruction volume, when assuming the shape of all blobs to be largely similar. The simultaneous distribution of particle intensity and size, as measured by the normalized Gamma, is shown in figure 4. The ghost and actual particle distributions are again partially overlapping, from which it is concluded that complete separation is difficult to achieve only having intensity and size information, as in non-time-resolved measurements. Hence one has to go to very low seeding densities when a complete ghost removal is required in those cases.

Returning to time-resolved measurements, the particle track length can be considered simultaneously with the particle size (figure 5). The ghosts that can be followed over the full volume length seem to have a size, i.e. normalized Gamma value, similar to actual particles. Combining particle size with track length information does not improve ghost detection.

Finally, particle intensity and track length are considered, which is found to effectively distinguish between ghosts and actual particles (figure 6). In the particle intensity-track length plane the actual particles are observed to fully separate from the ghosts, which allows removing all ghosts from the reconstructed volumes. In particular, the actual particles combine long tracks with high peak intensity, while a ghost can have either a high intensity or a long track, but never both. Before, Schröder et al. (2011) used separate thresholds on particle intensity and track length to remove potential ghost tracks. Here, we demonstrate the effectiveness of such an approach and show how thresholds may be selected in a more objective manner.

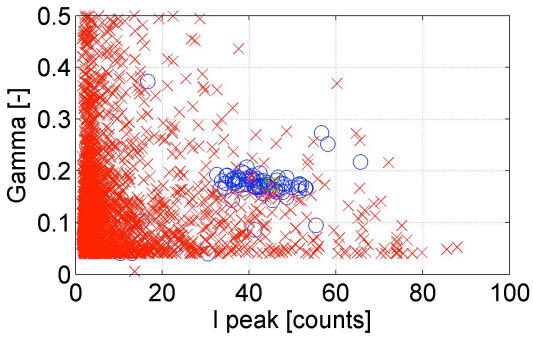

Figure 4. Simultaneous distribution of normalized Gamma and particle peak intensity. Results shown are for $ppp_{1D} = 0.07$ and $\theta = 0.5\%$. The red symbols (x) indicate ghost, the blue symbols (o) mark actual particles.

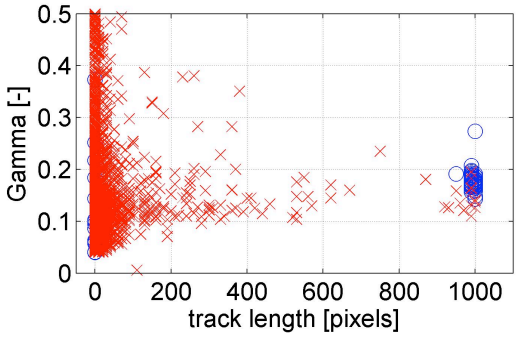

Figure 5. Simultaneous distribution of normalized Gamma and particle track length in voxels. Results shown are for $ppp_{1D} = 0.07$ and $\theta = 0.5\%$. The red symbols (x) indicate ghost, the blue symbols (o) mark actual particles.

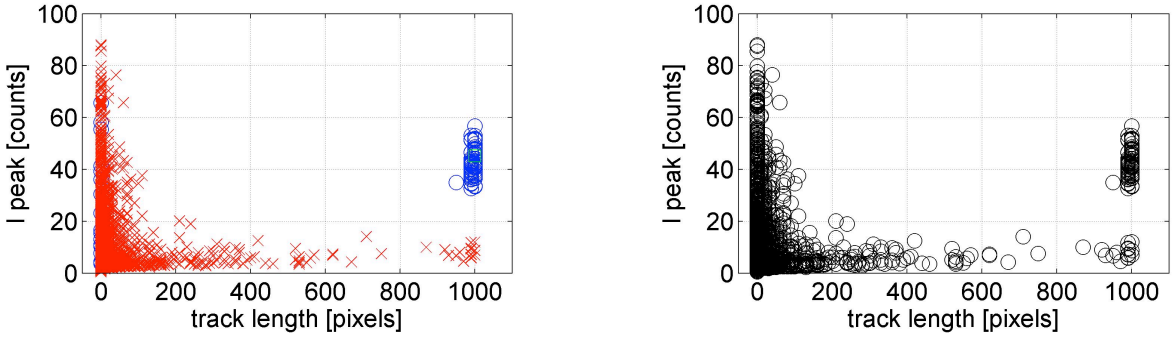

Figure 6. Simultaneous distribution of particle peak intensity and track length in voxels. Results shown are for $ppp_{1D} = 0.07$ and $\theta = 0.5\%$. (left) The red symbols (x) indicate ghost, the blue symbols (o) mark actual particles. (right) The same symbol is used for all particles to remove a possible observer bias and corresponding to the case when the location of the actual particles is unknown.

Furthermore, the particle intensity-track length plane can be used to examine whether all ghost can be removed in any particular experiment. This is illustrated in figure 7 considering different flow cases ranging from a uniform velocity fields, $\theta = 0.0\%$, up to a shear flow with $\theta = 5.0\%$. For low shear, $\theta = 0.0\%$ and 0.2%, the ghost distribution clearly tails to long track lengths with a concentration of tracks near the maximum of 1000 voxels. For $\theta = 0.2\%$ the ghost tail is seen to connect to the actual particles from the low particle intensity side. In that case, the ghosts and actual particles cannot be properly separated based on the point cloud in the particle intensity-track length plane alone. Note that a color-coding as used in these figures will not be available in an experiment. For $\theta = 0.0\%$ the actual particles show a slight separation from the ghosts, which is unexpected considering the variation in velocities across the volume is less than in the $\theta = 0.2\%$ case. However, the apparent gap is smaller than for $\theta = 0.5\%$ (figure 6) due to the expected intensity of the actual particles reducing from about 40 counts to 30 counts. Moreover, the present results are obtained from a limited time series, equivalent to following only 70 actual tracers over the full length of the measurement domain. Hence, the results are not statically converged and still depend on the exact details of how these individual particles are distributed in space. It thus appears that the gap between ghosts and actual particles in the $\theta = 0.0\%$ case is likely to close, as expected from the $\theta = 0.2\%$ result, when more data would be available. Increasing the velocity variation across the volume to $\theta = 2.0\%$ and 5.0%, results in shorter ghost track lengths and the ghost tail along the track length axis retracts. Still, the occasional ghost trajectory may stretch the full length of the volume, as for example in the $\theta = 5.0\%$ case, but its corresponding peak intensity will be much less than the actual particle intensity. These results signify that all ghost particles can be separated and removed when the tail near the track length axis (at low peak intensity) detaches from the cluster of points at long track lengths and at elevated intensity, corresponding to actual particles.

A similar analysis of the particle intensity-track length plane is carried out for increasing seeding densities, while keeping the shear flow constant at $\theta = 2.0\%$ (figure 8). The ghosts are found to detach from the actual particles between $ppp_{1D} = 0.10$ and 0.15. Furthermore, at the higher seeding density some tracks include both ghost and actual particles. This suggests particle trackability is reduced at that seeding density.

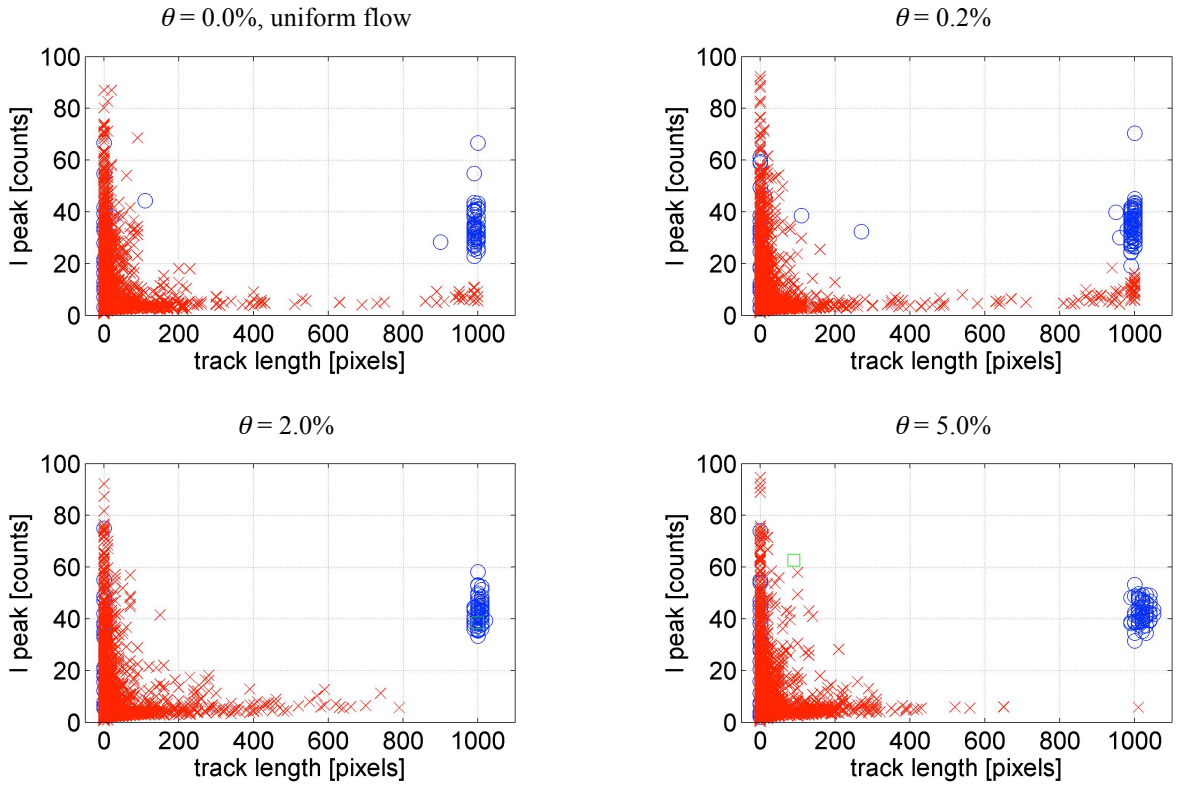

Figure 7. Effect of varying θ on the simultaneous distribution of particle peak intensity and track length in voxels. Results shown are for $ppp_{1D} = 0.07$. The red symbols (x) indicate ghost, the blue symbols (o) mark actual particles.

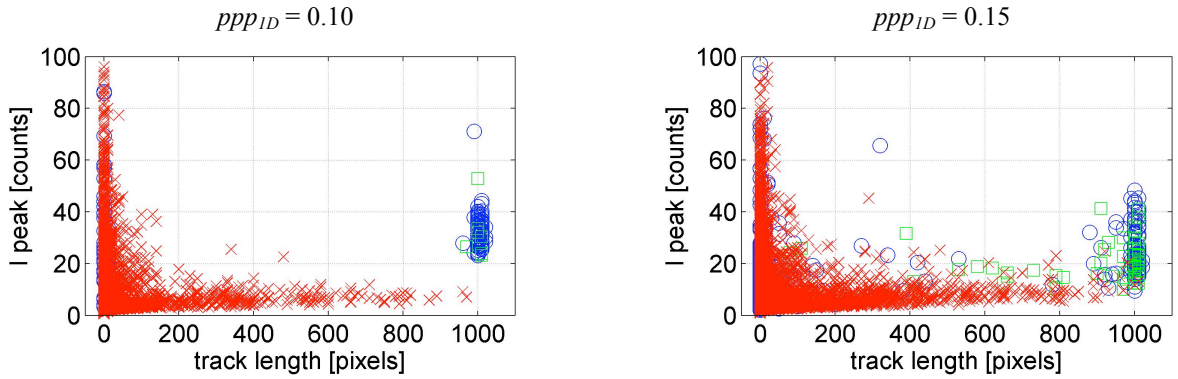

Figure 8. Effect of varying ppp_{1D} on the simultaneous distribution of particle peak intensity and track length in voxels. Results shown are for $\theta = 2.0\%$. The red symbols (x) indicate ghost, the blue symbols (o) mark actual particles, and the green symbols mark actual particle tracks, which include a ghost particle at only one time instant.

4. ULTIMATE MTE

The ghost detection method, proposed in the previous section, can further be used to remove these spurious intensity peaks from the reconstructed volumes and obtain an improved initial guess for following MART iterations. This may be considered an ultimate version of Motion Tracking Enhancement (MTE). Ultimate in the sense that it takes into account all available time information, 100 time steps presently, rather than just 2-7 steps (Novara et al. 2010, Novara 2013). The aim here is to investigate whether such a procedure significantly improves the accuracy of the reconstructed volumes and the particle tracking. And if so, does it increase the seeding density for which all ghosts can be separated from the actual particles in the particle intensity-track length plane?

This procedure is tested on the cases with $\theta = 2.0\%$ and varying ppp_{1D}. For the lower seeding densities ($ppp_{1D} = 0.07$ and 0.10) all ghosts separate from the actual particles in the particle intensity-track length plane (figure 7 and 8) and can, therefore, be detected without ambiguity. However, for $ppp_{1D} = 0.15$ such a separation does not occur and alternatively a threshold on the track length (800 voxels) is chosen as a detection criterion. All particles corresponding to tracks with a length below this threshold are considered to be ghost detections. The detected ghosts are removed from the volumes by setting the reconstructed intensity to zero within a radius of 2 voxels around the ghost peak location. To remove sharp transitions in the volume intensity distribution a Gaussian smooth (3x3 kernel) is applied subsequently. Starting from the cleaned volumes five more MART iterations are then performed.

The reconstruction quality is found to improve after applying ultimate-MTE-MART (table 1), as expected (Novara et al. 2010). Furthermore, the accuracy of the actual particle location in the reconstruction increases for the low seeding density cases ($ppp_{1D} = 0.07$ and 0.10), see table 2, which is consistent with decreasing random velocity error in MTE (Novara et al. 2010). Similar improvements in position error are reported for advanced tomographic algorithms like Iterative Particle Reconstruction (IPR, Wieneke 2013). In contrast, the particle position accuracy decreases by about 7% for the high seeding density $ppp_{1D} = 0.15$ case (table 2). Note that the net velocity accuracy in a measurement by cross-correlation may still improve due to fact that the noise contribution associated to ghosts has been reduced. This has not been verified yet.

Table 1. Improvements in reconstruction quality, Q, after removing ghosts and performing 5 additional MART iterations.

ppp_{1D}	Q	
	5 MART iterations	5 MART iterations followed by ghost removal and 5 additional MART iterations
0.07	0.90	0.94
0.10	0.84	0.91
0.15	0.72	0.79

Table 2. Improvements in the mean position error of the actual particles in the reconstruction (both directions combined), ε, after removing ghosts and performing 5 additional MART iterations.

ppp_{1D}	ε [voxels]	
	5 MART iterations	5 MART iterations followed by ghost removal and 5 additional MART iterations
0.07	0.23	0.16
0.10	0.30	0.18
0.15	0.45	0.48

If ghosts and actual particles are initially well separated ($ppp_{1D} = 0.07$ and 0.10 cases), then ultimate-MTE-MART can help to increase this separation in the particle intensity-track length plane, as shown in figure 9. The long actual particle tracks are unaffected, while the ghost trajectories decrease in length significantly. High intensity ghosts are found to remain mostly near the edges of the reconstruction. But if ghosts and actual particles are initially not well separated ($ppp_{1D} = 0.15$ case), ultimate-MTE-MART does not improve the result and in fact causes the actual particle tracks to break up into shorter tracks (figure 9). A second pass of ultimate-MTE-MART does not help and even increases the number of long ghost tracks with peak intensities comparable to the actual particles. MTE is counterproductive in that case, which is consisted with the increase in particle position error at $ppp_{1D} = 0.15$ (table 2). Therefore, it seems unlikely that a ghost removal approach with additional MART iterations will allow for a substantial increase in seeding density while maintaining an accurate particle tracking or a good ghost separation condition.

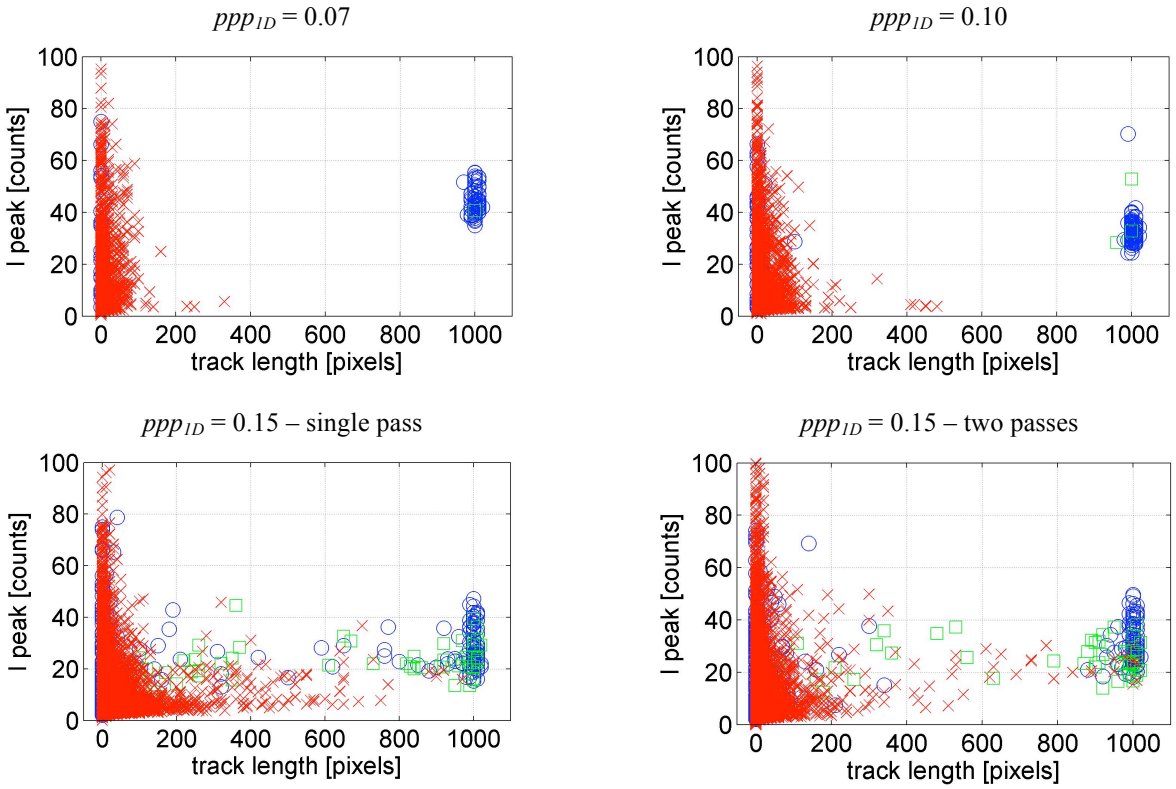

Figure 9. Effect of ghost removal in ultimate-MTE-MART on the simultaneous distribution of particle peak intensity and track length in voxels. Results shown are for varying ppp_{1D} and $\theta = 2.0\%$. The red symbols (x) indicate ghost, the blue symbols (o) mark actual particles, and the green symbols mark actual particle tracks, which include a ghost particle at only one time instant.

5. CONCLUSIONS

The properties of ghosts and actual particles in a tomographic reconstruction have been review based on numerical simulations of a time-resolved tomographic-PIV experiment. The flow under consideration was a linear shear flow. For each reconstructed particle, i.e. intensity peak, the following properties were determined: the peak intensity value, the peak width and the length over which these particles can be traced (referred to as track length). Peak intensity and track length were shown to have good discriminating power, that is, their expected value is different for ghost compared to actual particles. Still the corresponding distributions, i.e. pdf, overlap, which does not allow detection of all ghost particles by a single threshold. On the other hand, the size of the reconstructed particle did not reveal an important difference between ghosts and actual particles.

Simultaneous plotting of peak intensity and track length was shown to allow a complete separation of ghosts and actual particles. The latter appear as long tracks (track length equal to volume size) and relatively high peak intensity. The ghosts are scattered along the axes having either high intensity or long track lengths, but never both. Only at high seeding density and low velocity variation over the volume depth can long ghost tracks gain intensity and overlap with the actual particles in the particle intensity-track length plane.

In the particle intensity-track length plane, a ghost tail along the track-length axis disconnecting from the actual particles (i.e. long high intensity particle tracks) indicates all ghosts can be separated from the actual particles. Subsequent removal of these detected ghost from the reconstruction followed by additional MART iterations was shown to improve the reconstruction accuracy and reduce the error in the reconstructed location of the actual particles. However, when the ghosts do not fully separate from the actual particles in the particle intensity-track length plane, at higher seeding densities, (partial) ghost removal does improve reconstruction accuracy, but increases particle position errors and is observed to break up actual particle tracks into shorter trajectories indistinguishable from the ghost trajectories. Hence, such a ghost removal approach does not allow substantially increasing seeding density while maintaining particle tracking accuracy.

REFERENCES

Atkinson C and Soria J (2009) Efficient simultaneous reconstruction and direct cross-correlation techniques for tomographic particle image velocimetry (tomo-piv). *Exp. Fluids* **47**, 553-568

de Silva CM, Baidya R and Marusic I (2013) Enhancing Tomo-PIV reconstruction quality by reducing ghost particles. *Meas. Sci. Technol.* **24**, 024010

Elsinga GE, Scarano F, Wieneke B and van Oudheusden BW (2006a) Tomographic particle image velocimetry. *Exp. Fluids* **41**, 933-947

Elsinga GE, van Oudheusden BW and Scarano F (2006b) Experimental assessment of tomographic-PIV accuracy. In: *13th international symposium on applications of laser techniques to fluid mechanics*, Lisbon, Portugal

Elsinga GE, Westerweel J, Scarano F and Novara M (2011) On the velocity of ghost particles and the bias errors in tomographic-PIV. *Exp. Fluids* **50**, 825-838

La Porta A, Voth GA, Crawford AM, Alexander J and Bodenschatz E (2001) Fluid particle accelerations in fully developed turbulence. *Nature* **409**, 1017-1019

Maas HG, Gruen A and Papantoniou D (1993) Particle tracking velocimetry in three-dimensional flows. *Exp. Fluids* **15**, 133-146

Novara M, Batenburg KJ and Scarano F (2010) Motion tracking-enhanced MART for tomographic PIV. *Meas. Sci. Technol.* **21**, 035401

Novara M (2013) Advances in tomographic PIV. PhD thesis, Technische Universiteit Delft

Scarano F (2013) Tomographic PIV: principles and practice. *Meas. Sci. Technol.* **24**, 012001

Schröder A, Geisler R, Staack K, Elsinga GE, Scarano F, Wieneke B, Henning A, Poelma C and Westerweel J (2011) Eulerian and Lagrangian views of a turbulent boundary layer flow using time-resolved tomographic PIV. *Exp. Fluids* **50**, 1071–1091

Westerweel J, Elsinga GE and Adrian RJ (2013) Particle Image Velocimetry for Complex and Turbulent Flows, *Ann. Rev. Fluid Mech.* **45**, 409-436

Wieneke B (2013) Iterative reconstruction of volumetric particle distribution. *Meas. Sci. Technol.* **24**, 024008